

Electrochemical and Density Function Theory Investigations of L- Arginine as Corrosion Inhibitor for Steel in 3.5% NaCl

K. F. Khaled^{1,2,*} and Saedah R. Al-Mhyawi³

¹Materials and Corrosion Laboratory, Chemistry Department, Faculty of Science ,Taif University, Taif, Hawiya 888, Kingdom of Saudi Arabia

²Electrochemistry Research Laboratory, Chemistry Department, Faculty of Education, Ain Shams University, Roxy, Cairo, Egypt

³Department of Chemistry, Sciences Faculty for Girls, King Abdulaziz University, P.O. Box 2321. Jeddah 21451, Saudi Arabia

*E-mail: khaledrice2003@yahoo.com

Received: 30 December 2012 / *Accepted:* 29 January 2013 / *Published:* 1 March 2013

The corrosion inhibition effect of L-arginine has been used as corrosion inhibitor for steel in 3.5 % NaCl. In this study, electrochemical frequency modulation, EFM was used as an effective method for corrosion rate determination. In EFM measurements, corrosion current density was determined without prior knowledge of Tafel slopes. Corrosion rates obtained using EFM, were compared to that obtained from other chemical and electrochemical techniques. Data obtained from chemical and electrochemical measurements were in good agreement with the results obtained from EFM. Density functional theory (DFT) calculations have been used to investigate the adsorption of L-arginine molecule on steel surface.

Keywords: Steel; EIS ; Polarization; DFT; Neutral inhibition

1. INTRODUCTION

An important method of protecting materials against deterioration from corrosion is by using inhibitors. Unfortunately, many common corrosion inhibitors are health hazards for the inhibition of corrosion in aqueous heating and cooling systems [1-5]. There is a problem that many proven inhibitors with toxic properties include aromatic and nitrogen containing heterocyclic compounds, find applications in pickling processes and in the oil and gas industry [6-13]. To solve this problem, some researchers investigated the inhibition effect of environment-friendly inhibitors such as amino acids on metal corrosion [14-18]. At the present time there are more than 200 different amino acids known to

occur in nature. Most of the natural amino acids are the alpha amino acids which contain carboxyl and amino functionalities bonded to the same carbon atom.

In the literature, many studies have been devoted to corrosion (and inhibition) in acidic media in order to measure the corrosion rate or to identify the elementary processes. However, relatively few studies have been carried out in neutral media [19-25], probably because of the formation of insoluble corrosion products which adhere to the metal surface [26].

Interface inhibition presumes a strong interaction between the corroding substrate and the inhibitor [27, 28]. In this case, the inhibitor is potential-dependently adsorbed. The two-dimensional (2-D) adsorbate layer can affect the basic corrosion reactions in various ways which may be discussed in terms of the inhibition efficiency[29].

In the present work we report the results obtained in studying corrosion and corrosion inhibition of steel in aerated 3.5% NaCl solutions by L-arginine amino acid using dc measurements (potentiodynamic polarization) combined with ac measurements (electrochemical impedance spectroscopy and electrochemical frequency modulation) . The variation of the used techniques perfectly covered the way of corrosion of steel in the tested solution. Also, L-arginine has been reported as corrosion inhibitor for copper in acid medium[30] and is expected to be a good inhibitor for steel in 3.5 % NaCl due to the presence of a variety of donor groups in its structure. In addition, In this work, the adsorption behavior of L- arginine at steel surface will investigated by the molecule dynamics simulation method and density functional theory

2. EXPERIMENTAL DETAILS

The experiments were carried out using steel specimens with composition (C = 0.12 wt %, S = 0.04 wt %, Si = 0.015 wt %, Mn = 0.8 wt %, and Fe = balance).

A steel rod of the same composition was mounted in Teflon with an exposed area of 0.28 cm² used for potentiodynamic polarization, electrochemical impedance EIS, and electrochemical frequency modulation EFM measurements.

L-arginine was obtained from Aldrich chemical co. they were added to the corrosive medium (3.5 % NaCl) at concentrations of 100, 300, 700, 900 mg/l. In this study we choose 3.5 % NaCl in order to avoid the problems linked to the ohmic drop[31].

Prior to all measurements, the steel samples are abraded with a series of emery paper up to 0000 grit size. The specimens are washed thoroughly with bidistilled water degreased and dried with acetone.

Electrochemical experiments were carried out using a conventional electrolytic cell with three-electrode arrangement: saturated calomel reference electrode (SCE), platinum mesh as a counter electrode, and the working electrode (WE) had the form of a rod. The counter electrode was separated from the working electrode compartment by fritted glass. The reference electrode was connected to a Luggin capillary to minimize IR drop. Solutions were prepared from bidistilled water of the resistivity 13 MΩcm, Prior to each experiment, the specimen was polished with a series of emery papers of different grit sizes up to 0000 grit size, polished with Al₂O₃ (0.5 mm particle size), washed several

times with bidistilled water then with acetone and dried using a stream of air. The electrode potential was allowed to stabilize 60 minutes before starting the measurements. All experiments were conducted at 25 ± 1 °C.

Potentiodynamic polarization curves were obtained by changing the electrode potential automatically from (-700 to -250 mV vs SCE) at open circuit potential with scan rate of 0.1 mV s^{-1} .

EIS measurements were carried out in a frequency range of 100 kHz to 40 mHz with amplitude of 5 mV peak-to-peak using ac signals at open circuit potential.

Electrochemical frequency modulation, EFM, was carried out using two frequencies 2 Hz and 5 Hz. The base frequency was 1 Hz, so the waveform repeats after 1 second. The higher frequency must be at least two times the lower one. The higher frequency must also be sufficiently slow that the charging of the double layer does not contribute to the current response. Often, 10 Hz is a reasonable limit.

Measurements were performed with a Gamry Instrument Potentiostat/Galvanostat/ZRA. This includes a Gamry Framework system based on the ESA400, Gamry applications that include DC105 for dc corrosion measurements, EIS300 for electrochemical impedance spectroscopy measurements to calculate the corrosion current and the Tafel constants along with a computer for collecting the data. Echem Analyst 5.58 software was used for plotting, graphing and fitting data.

3. COMPUTATIONAL DETAILS

An adsorption phenomenon is of a key importance in understanding corrosion problems. Monte Carlo simulation techniques help in finding the preferential adsorption sites on iron surface through finding the low-energy adsorption sites or to investigate the preferential adsorption of mixtures of adsorbate components on iron surface. Materials studio 6.0, distributed by Accelrys, Inc. [32] has been used to build L-arginine molecule, iron surface and solvent molecules (water molecules). Molecular mechanics (force field) tools are used to investigate the simulated corrosion system. The key approximation in these studies that the potential energy surface, on which the atomic nuclei move, is represented by a classical force field, which are developed by parameterising data from experiment and high level quantum mechanical calculations. COMPASS force field stands for condensed-phase optimised molecular potentials for atomistic simulation studies [33], which is used to optimise the structures of all components of the corrosion system (iron substrate/solvent/inhibitor). It is the first ab initio force field that enables accurate and simultaneous prediction of chemical properties (structural, conformational, vibrational, etc.) and condensed-phase properties (equation of state, cohesive energies, etc.) for a broad range of chemical systems. It is also the first high-quality force field to consolidate parameters of organic and inorganic materials. The first step in this computational study is the preparation of a model of molecules, which will adsorb on the surface with optimised geometry (i.e. energy minimised). Among the different steps involved in the modelling approach is the construction of the iron surface from the pure crystal, the addition of the L-arginine molecule near to the surface, the definition of the potentials (i.e. the force field) to study the liquid–solid interaction, followed by the geometry optimization calculation.

This particular case, the use of molecular mechanics can be seen as a precursor to computationally more expensive quantum mechanical methods: Once the model has been optimised with suitable force field (COMPASS), we will be able to simulate a substrate (iron surface) loaded with an adsorbate (L-arginine molecules), taking into consideration the solvent effect. This computational study aims to find low-energy adsorption sites to investigate the preferential adsorption of L-arginine molecule on iron surface aiming to find a relation between the effect of its molecular structure and its inhibition efficiency. To build iron surface, amorphous cell module has been used to create solvent/L-arginine cell on iron surface. The behaviour of the L-arginine on the surface was studied using molecular dynamics simulations and the COMPASS force field. The MD simulation of the interaction between the L-arginine molecule dissolved in H₂O and the iron surface (111) was carried out in a simulation box (3.0 × 3.0 × 2.1 nm) with periodic boundary conditions in order to simulate a representative part of an interface devoid of any arbitrary boundary effects. A cut off distance of 1.0 nm with a spline switching function was applied for the non-bond interactions, i.e. for coulombic, van der Waals and hydrogen bond interactions. The cut off used to select the spline width, which specifies the size of the region within which nonbond interactions are splined from their full value to zero. For the actual computation of this interaction, energy charge groups are used. Cut off distance specifies the distance at which to exclude interactions from the nonbond list. The iron crystal is cleaved along with the (111) plane, thus representing the iron surface. For the MD simulation, all the spatial positions of the iron atoms in the simulation box are fixed because the thermal vibrations of the interaction with an adsorbed molecule and not in the physical behaviour of the crystal itself. The MD simulation simulates a substrate loaded with an adsorbate. A low-energy adsorption site is identified by carrying out a Monte Carlo search of the configurational space of the substrate–adsorbate system as the temperature is slowly decreased. This process is repeated to identify further local energy minima. During the course of the simulation, adsorbate molecule are randomly rotated and translated around the substrate. The configuration that results from one of these steps is accepted or rejected according to the selection rules of the Metropolis Monte Carlo method [34]. The force field used is COMPASS, charge is force field assigned, quality is fine and summation method is group- and atom based. All structures used in this study are minimised in order to ensure that the energy results used in calculating the adsorption energy are accurate; it is critically important that when we optimise the structures, we use the same energy minimization settings as we intend to use for calculating the adsorption energy of L-arginine. This includes not only the force field, atomic charges, and non-bond summation methods but also the quality of the energy and geometry optimization calculations and the convergence tolerances used for the minimization. Quantum chemical calculations carried out using Dewar's linear combinations of atomic orbitals–self-consistent field–molecular orbital (LCAO–SCF–MO) [35]. We used PM3 semi-empirical method in commercially available quantum chemical software Hyperchem, release 8.06 [36]. A full optimization of all geometrical variables without any symmetry constraint was performed at the restricted Hartree–Fock level. It develops the molecular orbitals on a valence basis set and also calculates electronic properties and the optimised geometries of the L-arginine molecules. As an optimization procedure, the built-in Polak–Ribiere algorithm was used [37].

4. RESULTS AND DISCUSSION

4.1 Electrochemical measurements

4.1.1 Electrochemical frequency modulation

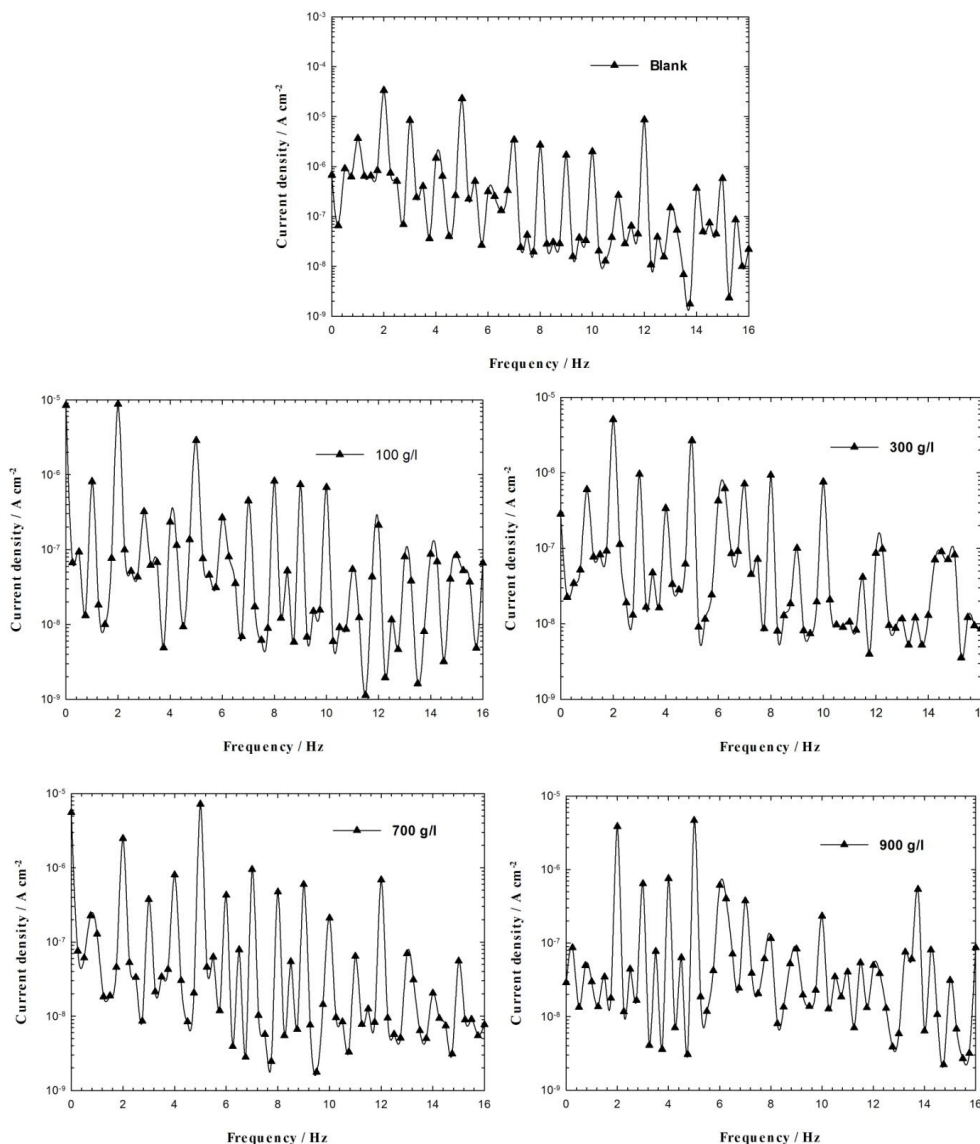


Figure 1. Intermodulation spectra for steel in 3.5 % NaCl in the absence and presence of various concentrations of L-arginine at 25 ± 1 °C.

The corrosion rate and Tafel parameters can be obtained with one measurement by analyzing the harmonic frequencies. Because current is a non-linear function of potential, the system responds in a non-linear way to the potential excitation. The current response contains the input frequencies, frequency components which are the sum, difference, and multiples of the two input frequencies.

The corrosion process is non-linear in nature, a potential distortion by one or more sine waves will generate responses at more frequencies than the frequencies of applied signal. Virtually no attention has been given to the intermodulation or electrochemical frequency modulation. However,

EFM showed that this non-linear response contains enough information about the corroding system so that the corrosion current can be calculated directly. The great strength of the EFM is the causality factors which serve as an internal check on the validity of the EFM measurement [38-41]. With the causality factors the experimental EFM data can be verified.

The results of EFM experiments are a spectrum of current response as a function of frequency. The spectrum is called the intermodulation spectrum and examples for corrosion of steel in absence and presence of L-arginine in 3.5% NaCl are shown in Fig. 1. The spectra contain current responses assigned for harmonical and intermodulation current peaks. The larger peaks were used to calculate the corrosion current density (i_{corr}), the Tafel slopes (b_c and b_a) and the causality factors (CF-2 and CF-3). These electrochemical parameters were simultaneously determined by Gamry EFM140 software, and listed in Table 1.

Table 1. Electrochemical kinetic parameters, inhibition efficiency recorded for steel in 3.5% NaCl solutions without and with various concentrations of L-arginine at 25 ± 1 °C calculated by EFM method

Conc. mg/l	i_{corr} $\mu\text{A.cm}^{-2}$	b_a mV.dec^{-1}	$-b_c$ mV.dec^{-1}	E_{EFM} %	C.F-2	C.F-3
0.00	112.3	100.7	138.2	-----	1.94	2.87
100	63.5	89.9	139.8	43.45	1.99	2.99
300	57.2	97.5	125.6	49.06	2.0	2.87
700	44.5	91.4	147.8	60.37	1.87	3.01
900	24.1	103.8	172.1	78.54	1.96	2.89

Inhibition efficiency (E_{EFM} %) presented in Table 1 calculated from the following equation.

$$E_{EFM} \% = \left(1 - \frac{i_{corr}}{i_{corr}^o}\right) \times 100 \quad (1)$$

where i_{corr}^o and i_{corr} are corrosion current density in the absence and presence of L-arginine, respectively.

Table 1 shows that the corrosion current densities decrease with increase in L-arginine concentrations. The standard values for CF-2 and CF-3 depicted in Table 1 are 2.0 and 3.0, respectively. The causality factor is calculated from the frequency spectrum of the current response. If the causality factors differ significantly from the theoretical values of 2.0 and 3.0, then it can be deduced that the measurements are influenced by noise. As the causality factors are approximately equal to the predicted values of 2.0 and 3.0 then there is a causal relationship between the perturbation signal and the response signal. Then the data are assumed to be reliable [42].

4.1.2 Electrochemical impedance spectroscopy

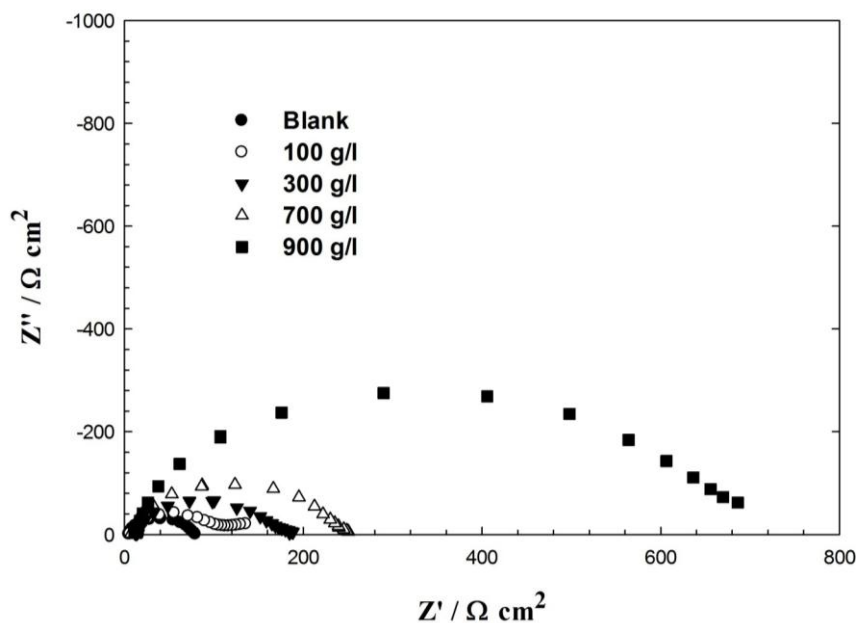


Figure 2. Measured complex plane impedance plots of steel corrosion in 3.5 % NaCl solutions at E_{corr} in the absence and presence of L-arginine at 25 ± 1 °C.

Impedance spectroscopy is a non-destructive technique and so can provide time dependent information about the properties but also about ongoing processes such as corrosion or any other electrochemical process. The usefulness of impedance spectroscopy lies in the ability to distinguish the dielectric and electric properties of individual contributions of components under investigation.

Table 2. Electrochemical parameters calculated from EIS measurements on steel electrode in 3.5 % NaCl solutions without and with various concentrations of L-arginine at 25 ± 1 °C.

Conc. mg/l	R_s $\square.cm^2$	R_p $\square.cm^2$	CPE $\mu\Omega^{-1}cm^{-2}S^n$	n	E_{IMP} %
0.00	2.3	79	38.1	0.78	-----
100	3.2	105.1	26.7	0.81	24.83
300	1.9	169.0	24.6	0.82	53.25
700	2.3	239.5	19.8	0.78	67.01
900	1.87	669.7	17.8	0.79	88.20

The results of the EIS measurements were presented in Fig. 2 as complex plane impedance plots. Impedance measurements were conducted in 3.5% NaCl solutions without and with different concentrations of the L-arginine. Complex-plane impedance plots presented in Fig. 2 showed depressed semicircle with the center under the real axis, such behaviour is characteristic for solid electrodes and often referred to as frequency dispersion and attributed to the roughness and other

inhomogeneities of the solid electrode [43-45]. The capacitive loop was related to charge-transfer in corrosion process [46]. The depressed form of the higher frequency loop reflects the surface inhomogeneity of structural or interfacial origin, such as those found in adsorption processes [47]. Complex-plane impedance plots presented in Fig. 2 are modeled using an equivalent circuit presented in Fig. 3, similar to the one proposed by several authors [48-50]

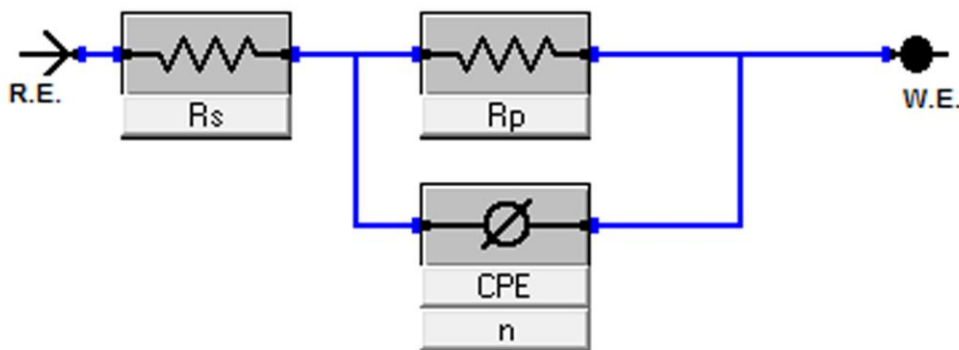


Figure 3. Equivalent circuit model for steel /NaCl interface

Parameters derived from equivalent circuit in Fig. 3 and inhibition efficiency is given in Table 2. By increasing the concentration of L-arginine, the values of polarization resistance increase and the CPE values is decreased. The constant phase element (CPE) with their n values $1 > n > 0$ represent double layer capacitors with some pores [51]. This decrease in (CPE) results from a decrease in local dielectric constant and/or an increase in the thickness of the double layer, suggested that L-arginine molecules inhibit the steel corrosion by adsorption at the steel/NaCl interface. The semicircles in Fig. 2 are generally associated with the relaxation of electrical double layer capacitors and the diameters of these semicircles can be considered as the charge-transfer resistance ($R_{ct} = R_p$) [52]. Therefore, the inhibition efficiency, $E_{IMP}\%$ of L-arginine for the steel electrode can be calculated from the charge-transfer resistance as follows [53]:

$$E_{IMP}\% = \left(1 - \frac{R_p^o}{R_p}\right) \times 100 \quad (2)$$

where R_p^o and R_p are the polarization resistances for uninhibited and inhibited solutions, respectively.

4.1.3 Potentiodynamic polarization

Measurements of current-potential values under carefully controlled conditions can yield information on corrosion rates, coatings and films, passivity, pitting tendencies and other important

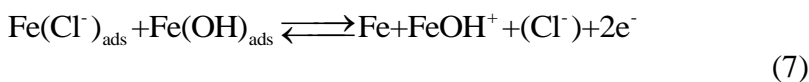
phenomena. It is well known that the cathodic reaction for metals in aerated neutral solutions is the oxygen reduction according to,



This process consumes the electrons that are released during the oxidation reaction, where the corrosion of iron can undergo two different transformations as follows



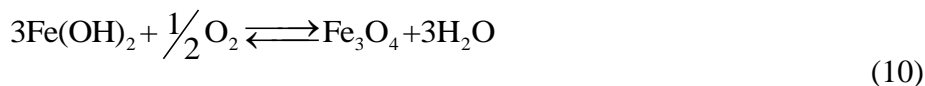
Nevertheless, in practice the second transformation, eq. (3), will not occur. While the dissolution of iron in concentrated NaCl solutions into ferrous cations can be explained according to Darwish et al. [54, 55]



In addition, the hydroxide ions resulting from equation 1 will react with $\text{Fe}_{\text{aq}}^{2+}$ to form a deposit of $\text{Fe}(\text{OH})_2$,



If there is an excess of oxygen presented, the formed ferrous hydroxide transforms to the final corrosion product that is called magnetite (Fe_3O_4) according to the following reaction,



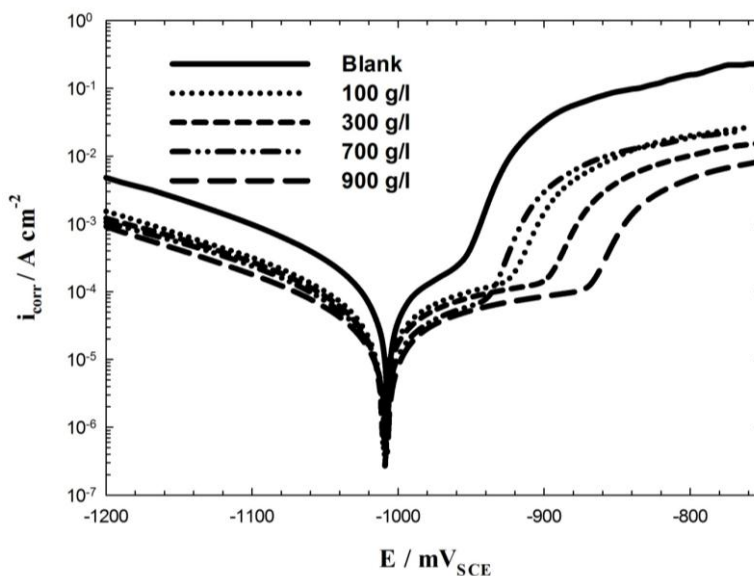


Figure 4. Anodic and cathodic Tafel polarization curves for mild steel in the absence and presence of various concentrations of L-arginine in 3.5% NaCl at 25 ± 1 °C.

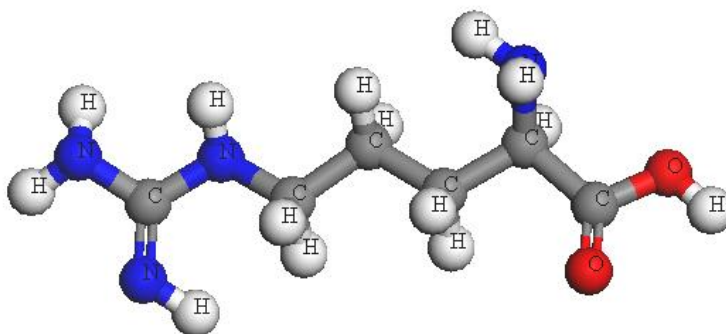


Figure 5. Geometry optimized structure of L-arginine molecule

Figure 4 shows the potentiodynamic polarization curves recorded for the steel electrode in the absence and presence of L-arginine are presented in Fig. 4. It is obvious from Fig. 4 that the polarization curve for iron, Fig. 4 shows a short active-passive region due to the dissolution of iron, as shown by equations 4, 5, 6, and 7, and the formation of corrosion products and/or oxide layers, as indicated by reaction (8) and reaction (9), respectively. At more positive potential values, the formed passive film dissolved due to the rapid increase of current of steel[55].

The cathodic reaction of steel in aerated sodium chloride solutions is well known to be the oxygen reduction (see eq. 1). Any corrosion processes that occur are usually a result of anodic currents.

It has been shown that in the Tafel extrapolation method, the use of both the anodic and cathodic Tafel regions is undoubtedly preferred over the use of only one Tafel region [56]. However, the corrosion rate can also be determined by Tafel extrapolation of either the cathodic or anodic polarization curve alone. If only one polarization curve is used, it is generally the cathodic curve which

usually produces a longer and better defined Tafel region. Anodic polarization may sometimes produce concentration effects, due to passivation and dissolution, as well as roughening of the surface which can lead to deviations from Tafel behaviour.

The cathodic curve is, therefore preferred over the anodic one for evaluation of corrosion currents, i_{corr} , by the Tafel extrapolation method. However, the anodic polarization curve deviate from the Tafel behaviour, exhibiting a limiting diffusion current, may be due to the reduction of dissolved oxygen. Accordingly, there is an uncertainty and source of error in the numerical values of the anodic Tafel slopes calculated by the software.

Addition of L-arginine reduces the cathodic and anodic currents, i_{corr} . The corresponding electrochemical kinetics parameters such as corrosion potential (E_{corr}), anodic Tafel slopes (b_a), cathodic Tafel slopes (b_c) and corrosion current density (i_{corr}), obtained by extrapolation of the Tafel lines are presented in Table 3.

Table 3. Electrochemical parameters calculated from polarization measurements on the steel electrode in 3.5 % NaCl solutions without and with various concentrations of L-arginine at 25 ± 1 °C.

Conc. mg/l	I_{corr} $\mu\text{A.cm}^{-2}$	$-E_{\text{corr}}$ mV	b_a mV.dec^{-1}	$-b_c$ mV.dec^{-1}	C.R mpy	E_T %
0.00	92.15	1007	68.6	109	39.53	----
100	66.82	1010	167.3	139.6	28.66	27.48
300	46.77	1009	161.6	129.4	20.06	49.24
700	36.94	1007	224.8	134.3	15.84	59.91
900	19.08	1008	73.74	111.3	8.18	79.29

The inhibitor efficiency E_T % was evaluated from dc measurements using the following equation [42]:

$$E_T \% = \left(1 - \frac{i_{\text{corr}}}{i_{\text{corr}}^0}\right) \times 100 \quad (11)$$

where i_{corr}^0 and i_{corr} correspond to uninhibited and inhibited current densities, respectively. E_T %.

4.2 Molecular level Study:

4.2.1 Simulated annealing

To simulate the iron surface (substrate) loaded with a set number of adsorbate molecules (L-arginine) the simulated annealing task is performed. By repeatedly searching the configurational space of the substrate-adsorbate system as the temperature is slowly decreased and then reset to the maximum through a number of temperature cycles, low energy adsorption sites are identified. L-

arginine molecules are confined to a defined adsorption region in the vicinity of the substrate such that the number of L-arginine molecules on the surface does not change. The Metropolis Monte Carlo method is used to search for adsorption configurations. In this method, only the positions and orientations of the L-arginine molecules are sampled; each conformation is treated as a rigid body. The Metropolis method assumes that the L-arginine molecules do not have a high degree of torsional flexibility and ignores any internal degrees of freedom that the L-arginine molecules may possess on the iron surface[57] .

Geometry optimization is based on reducing the magnitude of calculated force until they become smaller than defined convergence tolerances. The forces on an atom are calculated from the potential energy expression and will, therefore, depend on the forcefield that is selected. Geometry optimization is carried out for the studied system using an iterative process in which the atomic coordinates are adjusted until the total energy of a structure is minimized, i.e., it corresponds to a local minimum in the potential energy surface[57] [58].

The following algorithms which are available in Materials Studio software include (Steepest descent, Polak-Ribiere variant only, Quasi-Newton, Adjusted basis set Newton-Raphson, Smart) are used for geometry optimization. Different algorithms are better suited to certain circumstances, for example if the structure is far from equilibrium, it is best to use steepest descent. It is, therefore, often beneficial to combine algorithms in a cascade, such that, as the potential minimum is approached, a more appropriate method is used. The Smart algorithm is a cascade of the steepest descent, ABNR, and quasi-Newton methods[57] [58]. Figure 1 shows the geometry optimized structured for L-arginine molecule.

4.2.2 Metropolis Monte Carlo method

Using the Adsorption locator simulation module distributed by Accelrys, the L-arginine molecule – iron (111) configuration are sampled from a canonical ensemble. In the canonical ensemble, the loading of all L-arginine molecules on the iron (111) substrate, as well as the temperature, are fixed.

The probability of a configuration, m , in the canonical ensemble is given by equation 12[59]:

$$P_m = C e^{-\beta E_m} \quad (12)$$

where C is an arbitrary normalization constant, β is the reciprocal temperature, and E_m is the total energy of configuration m .

The reciprocal temperature is given by:

$$\beta = \frac{1}{k_B T} \quad (13)$$

where k_B is the Boltzmann constant and T is the absolute temperature.

The total energy of configuration m is calculated according to the following sum:

$$E_m = E_m^{AA} + E_m^{AS} + U_m^A \quad (14)$$

where E_m^{AA} is the intermolecular energy between the L-arginine molecules, E_m^{AS} is the interaction energy between the L-arginine molecules and the iron (111), and U_m^A is the total intramolecular energy of the L-arginine molecules. The intramolecular energy of the L-arginine is not included as its structure is fixed throughout the simulation; thus, this energy contribution is fixed and vanishes, since only energy differences play a role in Adsorption Locator calculations.

The total intramolecular energy, U^A , is the sum of the intramolecular energy of all adsorbates of all components:

$$U^A = \sum_{\{N\}_m} u_{intra} \quad (15)$$

Where $\{N\}_m$ denotes the set of adsorbate loadings of all components in configuration m .

An Adsorption Locator simulation always starts with a clean substrate. The first stage is to adsorb the specified number of L-arginine molecules. This is accomplished by a random series of insertion steps and equilibration moves (only moves that do not change the loading are permitted) until the specified loading has been reached. During this stage, only insertion steps that do not create structures with intermolecular close contacts and that pass all adsorbate location constraints are accepted[57].

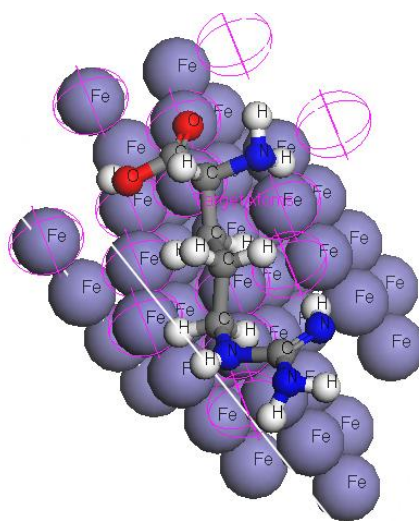


Figure 6. Most suitable configuration for adsorption of L-arginine on Fe(111) substrate obtained by adsorption locator module

The starting configuration will take several steps to adjust to the current temperature. A simulation is, therefore, separated into an equilibration and a production stage. The properties returned at the end of the run are based on the production stage only.

In the equilibration and production stages of an Adsorption Locator simulation, each step starts with the selection of a step type using the weights set at the start of the run. The step type can be either a translation or a rotation. After a step type is selected, a random component is chosen and the step type is applied to a random adsorbate of that component. The Metropolis Monte Carlo method is then used to decide whether to accept or reject the change.

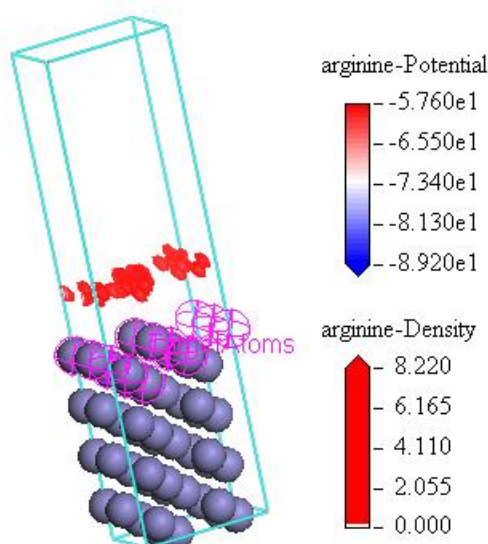


Figure 7. Adsorption density field of L-arginine on Fe(111) surface

The Metropolis Monte Carlo method in Adsorption Locator provides four step types for a canonical ensemble: conformer, rotation, translation, and regrowth[60]. Figure 6 shows the most suitable L-arginine conformation adsorbed on Fe(111) substrate obtained by adsorption locator module[34, 61, 62]. The adsorption density of L-arginine on the Fe(111) substrate has been presented in Fig. 7. As can be seen from Figs. 6 and 7 that the L-arginine molecule shows ability to adsorb on Fe surface. Also, it has high binding energy to Fe surface as seen in Table 4. The outputs and descriptors calculated by the Monte Carlo simulation are presented in Table 4. The parameters presented in Table 4 include total energy, in kJ mol^{-1} , of the substrate–adsorbate configuration. The total energy is defined as the sum of the energies of the adsorbate components, the rigid adsorption energy and the deformation energy. In this study, the substrate energy (iron surface) is taken as zero. In addition, adsorption energy in kJ mol^{-1} , reports energy released (or required) when the relaxed adsorbate components (L-arginine in H_2O) are adsorbed on the substrate. The adsorption energy is defined as the sum of the rigid adsorption energy and the deformation energy for the adsorbate components. The rigid adsorption energy reports the energy, in kJ mol^{-1} , released (or required) when the unrelaxed adsorbate components (i.e., before the geometry optimization step) are adsorbed on the substrate. The

deformation energy reports the energy, in kJ mol^{-1} , released when the adsorbed adsorbate components are relaxed on the substrate surface.

Table 4. The output and descriptors calculated by the Monte Carlo simulation of L-arginine confirmations on iron (111) surface

Structures	Total energy	Adsorption energy	Rigid adsorption energy	Deformation energy	L-arginine dE_{ad}/dN_i	Calculated binding Energy
Fe (1 1 1) - 1	-835.66	-374.62	-404.97	30.34	-374.62	710.64
Fe (1 1 1) - 2	-815.89	-354.86	-384.83	29.97	-354.86	702.66
Fe (1 1 1) - 3	-813.03	-352.00	-368.71	16.70	-352.00	700.56
Fe (1 1 1) - 4	-806.11	-345.08	-352.74	7.663	-345.08	697.62
Fe (1 1 1) - 5	-797.62	-336.59	-351.54	14.95	-336.59	687.54
Fe (1 1 1) - 6	-794.56	-333.53	-342.22	8.692	-333.53	672.84
Fe (1 1 1) - 7	-782.76	-321.73	-350.14	28.41	-321.73	661.92
Fe (1 1 1) - 8	-781.44	-320.41	-326.74	6.331	-320.41	646.38
Fe (1 1 1) - 9	-775.56	-314.53	-357.93	43.39	-314.53	629.16
Fe (1 1 1) - 10	-773.36	-312.33	-359.51	47.18	-312.33	564.06
Fe (1 1 1) - 11	-769.40	-308.36	-368.82	60.45	-308.36	559.02
Fe (1 1 1) - 12	-755.16	-294.12	-331.51	37.38	-294.12	541.38
Fe (1 1 1) - 13	-718.31	-257.28	-264.19	6.912	-257.28	536.76
Fe (1 1 1) - 14	-716.05	-255.02	-263.87	8.849	-255.02	529.62
Fe (1 1 1) - 15	-702.93	-241.90	-262.26	20.35	-241.90	509.04

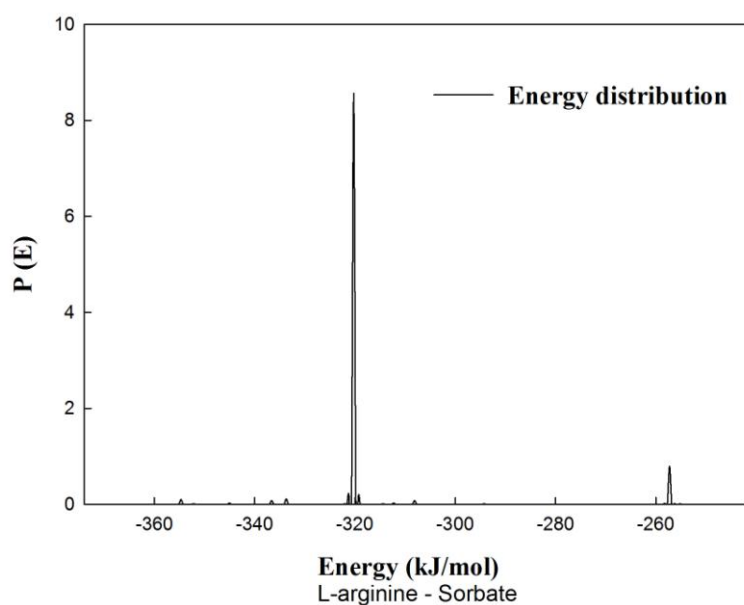


Figure 8. The adsorption energy distribution of the adsorbate (L-arginine) on iron (111) surface.

Table 1 shows also (dE_{ads}/dN_i) , which reports the energy, in kJ mol^{-1} , of substrate–adsorbate configurations where one of the adsorbate components has been removed. The binding energy introduced in Table 1 calculated from equation 16

$$E_{\text{binding}} = E_{\text{total}} - (E_{\text{surface}} + E_{\text{inhibitor}}) \quad (16)$$

Where E_{total} is the total energy of the surface and inhibitor, E_{surface} is the energy of the Fe (111) surface without the inhibitor, and $E_{\text{inhibitor}}$ is the energy of the inhibitor without the surface.

Figure 8 shows the adsorption energy distribution of the L-arginine molecules on Fe (1 1 1). As can be seen in Fig. 8, the adsorption energy of L-arginine reaches $(-89.19 \text{ KJ mole}^{-1})$ which shows the adsorption power for L-arginine molecules on iron (111) surface.

5. CONCLUSION

The main conclusions of the present study can be summarized as follows:

- The electrochemical measurements demonstrated that L-arginine acts as good inhibitor for steel corrosion in 3.5% NaCl solutions.
- EFM can be used as a rapid and non destructive technique for corrosion rate measurements without prior knowledge of Tafel constants.
- The results of EIS indicate that the value of CPEs tends to decrease and both charge transfer resistance and inhibition efficiency tend to increase by increasing the inhibitor concentration.
- Tafel polarization studies have shown that the L-arginine amino acid affects both the cathodic and anodic processes and thus it acts as mixed-type inhibitor.
- Computational studies help to find the most stable inhibitor conformation and adsorption sites for a broad range of materials. This information can help to gain further insight about corrosion system, such as the most likely point of attack for corrosion on a surface, the most stable site for inhibitor adsorption, adsorption density of the inhibitor and the binding energy of the adsorbed layer.

ACKNOWLEDGMENTS

Authors would like to thank King Abdul Aziz City for Science and Technology, KACST for the financial support of this work provided through project # AT-30-66 titled " Development of a new corrosion protection strategy for water-ammonia refrigerating systems ".

References

1. M.C. Lafont, N. Pebere, F. Morin, P. Bleriot, *Revue des Sciences de l'etat*, 6 (1993) 97.
2. L. Herrag, M. Bouklah, N.S. Patel, B.M. Mistry, B. Hammouti, S. Elkadiri, M. Bouachrine, *Res. Chem. Intermed.*, 38 (2012) 1669-1690.
3. K. Barouni, L. Bazzi, R. Salghi, M. Mihit, B. Hammouti, A. Albourine, S. El Issami, *Mater. Lett.*,

- 62 (2008) 3325-3327.
4. D.-Q. Zhang, H. Wu, L.-X. Gao, *Mater. Chem. Phys.*, 133 (2012) 981-986.
 5. K.F. Khaled, *Mater. Chem. Phys.*, 112 (2008) 290-300.
 6. K. Khaled, *Mater. Chem. Phys.*, 125 (2011) 427-433.
 7. G. Brunoro, F. Zucchi, M. Zucchini, *Materials Chemistry*, 5 (1980) 135-145.
 8. F. Mansfeld, M.W. Kendig, W.J. Lorenz, *J. Electrochem. Soc.*, 132 (1985) 290-296.
 9. K.F. Khaled, *J. Electrochem. Soc.*, 158 (2011) S28-S28.
 10. K.F. Khaled, *J. Electrochem. Soc.*, 157 (2010) C116-C124.
 11. K.F. Khaled, M.N.H. Hamed, K.M. Abdel-Azim, N.S. Abdelshafi, *J. Solid State Electrochem.*, 15 (2011) 663-673.
 12. R.D. Armstrong, A.C. Coates, *Journal of Electroanalytical Chemistry and Interfacial Electrochemistry*, 50 (1974) 303-313.
 13. A.S. Raja, S. Rajendran, P. Satyabama, *Journal of Chemistry*, (2013).
 14. P. Mohan, R. Usha, G.P. Kalaignan, V.S. Muralidharan, *Journal of Chemistry*, (2013).
 15. M.J. Firdhouse, D. Nalini, *Journal of Chemistry*, (2013).
 16. H. Ma, S. Chen, L. Niu, S. Zhao, S. Li, D. Li, *J. Appl. Electrochem.*, 32 (2002) 65-72.
 17. K.F. Khaled, *J. Appl. Electrochem.*, 39 (2009) 429-438.
 18. Zarrouk, B. Hammouti, H. Zarrok, M. Bouachrine, K.F. Khaled, S.S. Al-Deyab, *Int. J. Electrochem. Sci*, 7 (2012) 89-105.
 19. E.-S.M. Sherif, *Int. J. Electrochem. Sci*, 6 (2011) 3077-3092.
 20. R.T. Loto, C.A. Loto, A.P.I. Popoola, *Int. J. Electrochem. Sci*, 7 (2012) 7016-7032.
 21. K.F. Khaled, N.A. Al-Mobarak, *Int. J. Electrochem. Sci*, 7 (2012) 1045-1059.
 22. K.F. Khaled, N.S. Abdelshafi, A.A. Elmaghraby, A. Aouniti, N.A. Almobarak, B. Hammouti, *Int. J. Electrochem. Sci*, 7 (2012) in press.
 23. K.F. Khaled, N.S. Abdelshafi, A. El-Maghraby, A. Aouniti, N. Al-Mobarak, B. Hammouti, *Int. J. Electrochem. Sci*, 7 (2012) 12706 - 12719.
 24. K.F. Khaled, N.S. Abdel-Shafi, N.A. Al-Mobarak, *Int. J. Electrochem. Sci*, 7 (2012) 1027-1044.
 25. K. Khaled, N. Abdel-Shafi, N. Al-Mobarak, *Int. J. Electrochem. Sci*, 7 (2012) 1027-1044.
 26. E.M. Sherif, S.M. Park, *Electrochim. Acta*, 51 (2006) 1313-1321.
 27. S. Ramesh, S. Rajeswari, *Electrochim. Acta*, 49 (2004) 811-820.
 28. T.H. Muster, H. Sullivan, D. Lau, D.L.J. Alexander, N. Sherman, S.J. Garcia, T.G. Harvey, T.A. Markley, A.E. Hughes, P.A. Corrigan, A.M. Glenn, P.A. White, S.G. Hardin, J. Mardel, J.M.C. Mol, *Electrochim. Acta*, 67 (2012) 95-103.
 29. W.J. Lorenz, F. Mansfeld, *Electrochim. Acta*, 31 (1986) 467-476.
 30. N.A. Darwish, F. Hilbert, W.J. Lorenz, H. Rosswag, *Electrochim. Acta*, 18 (1973) 421-425.
 31. J.O.M. Bockris, M.A. Genshaw, V. Brusica, H. Wroblowa, *Electrochim. Acta*, 16 (1971) 1859-1894.
 32. L.M. Baugh, *Electrochim. Acta*, 24 (1979) 657-667.
 33. H. Ashassi-Sorkhabi, N. Ghalebsaz-Jeddi, F. Hashemaddeh, H. Jahani, *Electrochim. Acta*, 51 (2006) 3848-3854.
 34. J. Zhang, *Corros. Sci.*, 51 (2009) 1207-1227.
 35. J.S. Warner, R.P. Gangloff, *Corros. Sci.*, 62 (2012) 11-21.
 36. Y. Tan, *Corros. Sci.*, 53 (2011) 1845-1864.
 37. Y. Tan, *Corros. Sci.*, 53 (2011) 1145-1155.
 38. H. Tamura, *Corros. Sci.*, 50 (2008) 1872-1883.
 39. C.G. Soares, Y. Garbatov, A. Zayed, G. Wang, *Corros. Sci.*, 51 (2009) 2014-2026.
 40. Z. Shi, A. Atrens, *Corros. Sci.*, 53 (2011) 226-246.
 41. B.W.A. Sherar, P.G. Keech, D.W. Shoesmith, *Corros. Sci.*, 66 (2013) 256-262.
 42. F. Mert, C. Blawert, K.U. Kainer, N. Hort, *Corros. Sci.*, 65 (2012) 145-151.
 43. M. Kermani, J.C. Scully, *Corros. Sci.*, 19 (1979) 111-122.

44. S. Joshi, E.A. Kulp, W.G. Fahrenholtz, M.J. O'Keefe, *Corros. Sci.*, 60 (2012) 290-295.
45. M. Heydari, M. Javidi, *Corros. Sci.*, 61 (2012) 148-155.
46. L. Han, S. Song, *Corros. Sci.*, 50 (2008) 1551-1557.
47. C. Guedes Soares, Y. Garbatov, A. Zayed, G. Wang, *Corros. Sci.*, 50 (2008) 3095-3106.
48. M.T. Gudze, R.E. Melchers, *Corros. Sci.*, 50 (2008) 3296-3307.
49. R.S. Gonçalves, D.S. Azambuja, A.M. Serpa Lucho, *Corros. Sci.*, 44 (2002) 467-479.
50. G. Gece, *Corros. Sci.*, 53 (2011) 3873-3898.
51. D. de la Fuente, I. Díaz, J. Simancas, B. Chico, M. Morcillo, *Corros. Sci.*, 53 (2011) 604-617.
52. D.D. MacDonald, B.C. Syrett, S.S. Wing, *Corrosion*, 34 (1978) 289.
53. A.S. Fouda, M. Abdallah, A.M. Atya, H.D. Sabaa, *Corrosion*, 68 (2012) 610-619.
54. R.W. Bosch, F. Moons, J.H. Zheng, W.F. Bogaerts, *Corrosion*, 57 (2001) 532-539.
55. M. Mitzlaff, H.N. Hoffmann, K. Juettner, W.J. Lorenz, *Phys. Chem. Chem. Phys.*, 92 (1988) 1234-1244.
56. K.F. Khaled, S.S. Abdel-Rehim, G.B. Sakr, *Arabian Journal of Chemistry*, 5 (2012) 213-218.
57. K.F. Khaled, S.S. Abdel-Rehim, G.B. Sakr, *Arabian Journal of Chemistry*, 5 (2012) 213-218.
58. O. Olivares-Xometl, N.V. Likhanova, M.A. Domínguez-Aguilar, J.M. Hallen, L.S. Zamudio, E. Arce, *Appl. Surf. Sci.*, 252 (2006) 2139-2152.
59. L. Niu, H. Zhang, F. Wei, S. Wu, X. Cao, P. Liu, *Appl. Surf. Sci.*, 252 (2005) 1634-1642.
60. Z. Ghasemi, A. Tizpar, *Appl. Surf. Sci.*, 252 (2006) 3667-3672.
61. H. Ashassi-Sorkhabi, M.R. Majidi, K. Seyyedi, *Appl. Surf. Sci.*, 225 (2004) 176-185.
62. H. Ashassi-Sorkhabi, Z. Ghasemi, D. Seifzadeh, *Appl. Surf. Sci.*, 249 (2005) 408-418.